

# TeO<sub>2</sub> nanoparticles synthesized by evaporation of tellurium in atmospheric microwave-plasma torch-flame

Soon Cheon Cho, Yong Cheol Hong, Han Sup Uhm \*

*Department of Molecular Science and Technology, Ajou University, San 5, Wonchon-Dong, Youngtong-Gu, Suwon 443-749, Republic of Korea*

Received 23 June 2006; in final form 27 July 2006

Available online 9 August 2006

## Abstract

Tellurium dioxide (TeO<sub>2</sub>) nanoparticles were synthesized directly by evaporation of tellurium (Te) granules in an atmospheric microwave-plasma torch-flame with possibility for a direct continuous preparation and mass production of TeO<sub>2</sub> nanoparticles. The mean size of the synthesized TeO<sub>2</sub> particles was 108.2 nm observed from the TEM image and was 112.0 nm estimated by the Williamson–Hall plot using XRD data. The surface area and pore distribution properties of the particles were also analyzed by making use of a nitrogen adsorption apparatus.

© 2006 Elsevier B.V. All rights reserved.

The tellurium dioxide (TeO<sub>2</sub>) nanoparticles have attracted much attention lately both in fundamental and application research areas [1–3], because TeO<sub>2</sub> have various outstanding physical properties. For example, TeO<sub>2</sub>-based glasses manifest remarkable dielectric properties including very high hyper-polarization [4]. Also, TeO<sub>2</sub> glasses are less hygroscopic than borate and phosphate glasses [5,6]. The TeO<sub>2</sub>-based glasses are also very promising for non-linear optical device due to their high non-linear refractive indices, which could be 100 times more than that of SiO<sub>2</sub> [7]. So far, pure tellurium oxide glasses present the highest non-linear index. However, it is very difficult to obtain TeO<sub>2</sub> glasses under conventional process of melting and air-quenching mechanism. Only small amounts of pure TeO<sub>2</sub> glass and powder samples have been successfully prepared by melting it at 800 °C and then quenching it in a freezing mixture consisted of ice, ethanol and NaCl at temperatures less than –11 °C [8]. Therefore, the sol–gel process has been investigated in order to produce pure TeO<sub>2</sub> amorphous materials at low temperature, without melting mechanism. Until now, only few investigative researches of sol–gel process have been done. However, Hodgson

and Weng [9] have found the conditions to produce TeO<sub>2</sub> powders from tellurium alkoxides by precipitation.

In this Letter, we present a simple method for the synthesis of TeO<sub>2</sub> nanoparticles by directly heating Tellurium (Te) granule samples in an oxygen microwave-plasma torch-flame at atmospheric pressure. Atmospheric microwave plasmas generally produce a high-temperature plasma flame due to ohmic heating by high frequency electric fields, revealing a maximum central temperature of 6500 ± 350 K [10] and atomic and molecular oxygen of high density [11]. Therefore, from the synthesis standpoint of nanoparticles, such characteristics are favorable to instantaneously evaporate metal and explosively oxidize metal vapors. We also remind the reader that there is no earlier research work for synthesis of TeO<sub>2</sub> nanoparticles by directly heating Te granule samples in the microwave plasma flame.

A schematic diagram for the preparation of TeO<sub>2</sub> nanoparticles is shown in Fig. 1. The microwave synthesis system has been presented elsewhere [12–16]. As shown in Fig. 1, the synthesis system of TeO<sub>2</sub> nanoparticles consists mainly of the microwave plasma torch operated at 2.45 GHz and gas feeders controlled by mass flow controllers (MFCs). A microwave generator supplies the reactive energy to the flowing gas at the atmospheric pressure. An efficient power transfer through the microwave from the

\* Corresponding author. Fax: +82 31 219 2969.

E-mail address: [hsuhm@ajou.ac.kr](mailto:hsuhm@ajou.ac.kr) (H.S. Uhm).

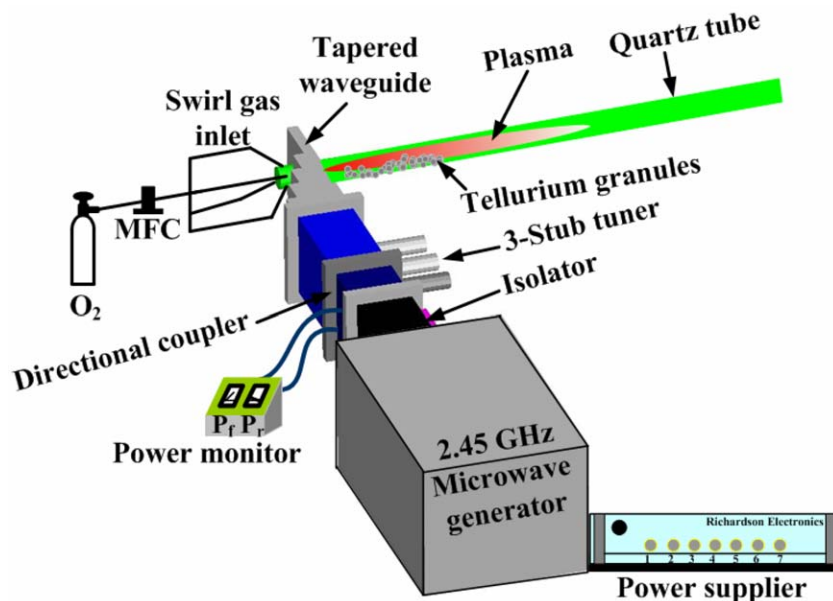


Fig. 1. Schematic diagram showing the experimental set-up for preparation of  $\text{TeO}_2$  nanoparticles by  $\text{O}_2$  microwave plasma flame.

microwave generator to the reactive gas is achieved through a matching network, which basically consists of an isolator, directional coupler, and three stub tuner. The center axis of quartz tube (170 mm inner diameter, 1.5 mm thickness, and 500 mm length) is located at  $1/4$  wavelength from the short end of the waveguide where the induced electric field is peaked before the plasma is initiated and is perpendicular to the wide waveguide walls. The plasma initiation is accomplished by inserting a tungsten wire into the quartz tube in the waveguide and sparking in it. The microwave-induced electric field inside the quartz tube can be maximized by adjusting the three stub tuner. This produces a plasma torch with high temperature ( $6500 \pm 350$  K) and high plasma density ( $\sim 10^{13}/\text{cm}^3$ ). Therefore, the microwave plasma torch provides a highly unusual and reactive chemical environment in which several plasma-molecular reactions occur.

Fifteen liters per minute (lpm)  $\text{O}_2$  as a swirl gas injected to the tangential direction of the quartz tube upstream via four small holes (swirl gas inlets) in Fig. 1 keeps the plasma flame off the inside walls of the quartz tube, confining the plasma to the center of the tube. In other words,  $\text{O}_2$  swirl gas plays pivotal roles not only in plasma stabilization by vortex flows but also in chemical reactions by providing radicals and ions. Te granules (99.9%, Aldrich) of 2 mm average size were placed inside the quartz tube, in which a high-temperature oxygen plasma flame is generated. Actually, as the swirl gas flow increases, the diameter and length of the microwave plasma decrease [16]. Fifteen lpm  $\text{O}_2$  as a swirl gas was injected into the microwave plasma torch initiated. Te granules placed inside the quartz tube are not in contact with the plasma torch-flame generated at flow rate of 15 lpm  $\text{O}_2$  and do not melt yet. Remember that Te has a melting point of  $\sim 722$  K and a boiling point of  $\sim 1263$  K. However, when  $\text{O}_2$  flow rate decreases

to 5 lpm, the length and diameter of the plasma torch-flame increases and then an explosive oxidation reaction of Te occurs owing to the contact between Te granules and the plasma torch-flame. Namely, Te granules in solid melt immediately and are vaporized by the  $\text{O}_2$  microwave-plasma torch-flame. The  $\text{TeO}_2$  nanoparticles are synthesized by oxidation reactions of the Te vapors and oxygen radicals ( $\text{O}^*$ ) produced in pure  $\text{O}_2$  plasma. It may take a few seconds that  $\text{TeO}_2$  nanoparticles are formed in the microwave plasma torch and are deposited in the inner wall of the quartz tube.

X-ray diffraction (XRD) patterns were obtained on a RIGAKU 12KW diffractometer, using  $\text{Cu K}\alpha$  radiation at a scan rate of  $0.02^\circ 2\theta \text{ s}^{-1}$ . In order to observe the surface morphology and structure of our samples obtained, a scanning electron microscope (SEM) and a transmission electron microscopy (TEM) were employed. The Brunauer–Emmett–Teller (BET) surface area of the as-produced sample was analyzed by nitrogen adsorption in a Micromeritics ASAP 2010 nitrogen adsorption apparatus. The BET surface area was determined by the multipoint BET method using the adsorption data. The pore size distribution from the desorption branch of the isotherm was calculated, according to the method developed by Barrett–Joyner–Halender (BJH) [17].

Fig. 2 shows the selected time sequence images of the plasma emission color during the synthesis of  $\text{TeO}_2$  nanoparticles. The images were captured by a digital camera at 16 Hz frame rate. Fig. 2a is the picture of microwave plasma operated at 15 lpm  $\text{O}_2$  and 1 kW plasma power. Once the synthesis of  $\text{TeO}_2$  nanoparticles starts by the contact between Te granules and the plasma flame, as shown in Fig. 2b–e, a pale blue light like a flesh is emitted from the torch flame. Fig. 2f shows the deposits inside the quartz tube after synthesis finish, revealing a typical  $\text{TeO}_2$  powder.

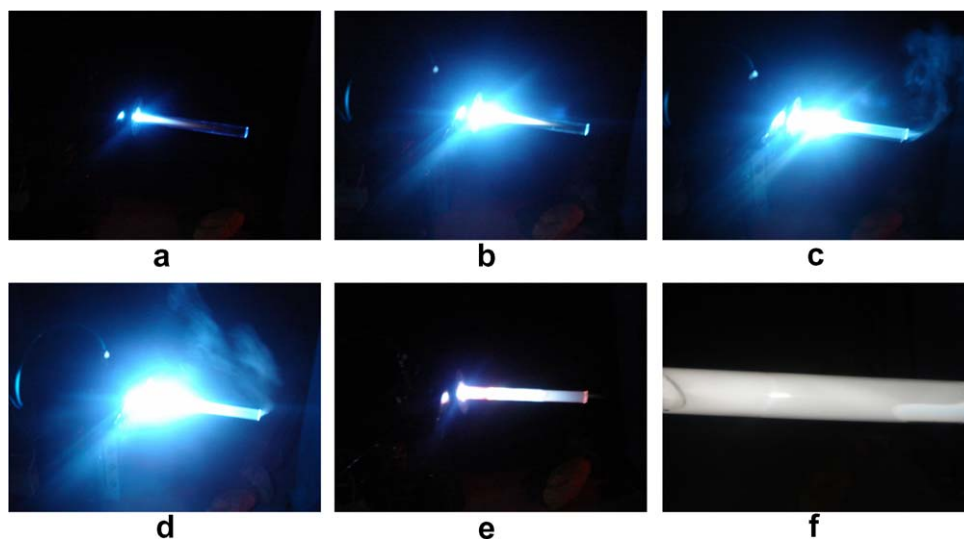


Fig. 2. Selected time-sequence images of the color of the microwave-plasma torch-flame during the synthesis of  $\text{TeO}_2$ : (a) Plasma flame at 15 lpm  $\text{O}_2$  and 1 kW plasma power. (b–e) Plasma emissions showing explosive oxidation-reactions between plasma and Te species. (f) Deposits inside the quartz tube after synthesis finish. (For interpretation of the references to color in this figure legend, the reader is referred to the web version of this article.)

All the XRD reflections in Fig. 3a can be indexed to the standard powder pattern for the pure sphere phase of  $\text{TeO}_2$  [space group:  $p4_12_12$  (92)] with lattice constants  $a = 4.808 \text{ \AA}$ ,  $c = 7.612 \text{ \AA}$ , which are in good agreement with the reported data (JCPDS file No. 84-1777) [18]. Apart from a small peak of residual Te in Fig. 3a, most of the Te granules close to 100% were converted to  $\text{TeO}_2$ . The strong intensities relative to the background signal indicate the high purity of the  $\text{TeO}_2$  sphere phase of the resulting products. The Williamson–Hall method [19] can be used to determine the crystallite size and lattice strain when there are three more reflections available for measurement. Contributions of the crystallite size and lattice strain are given by the following equation:

$$\beta \cos \theta = \frac{k\lambda}{L} + \eta \sin \theta \quad (1)$$

where  $\lambda$  is the wavelength of the X-rays ( $\lambda = 1.54 \text{ \AA}$  in this experiment),  $\theta$  is the diffraction angle,  $\eta$  is the lattice strain,  $L$  is the crystallite size,  $k$  is a constant (0.94 for GAUSSIAN line profiles and small cubic crystals of uniform size), and  $\beta$  is the full width at half maximum (FWHM). In Eq. (1), a plot of  $\beta \cos \theta$  vs  $\sin \theta$  yields a straight line with a slope  $\eta$  and intercept of  $k\lambda/L$ . Fig. 3b shows a Williamson–Hall plot using XRD data in Fig. 3a. The crystallite size was determined to be approximately 112 nm from the intercept in Fig. 3b and the almost flat slope indicates minimal strain ( $\eta = 1.3 \times 10^{-3}$ ) in the powder.

The SEM image in Fig. 4a shows a group of the  $\text{TeO}_2$  clusters aggregated with several particles composed of a few hundreds of nanometers in size. The aggregates were made in the plasma region due to a high-temperature

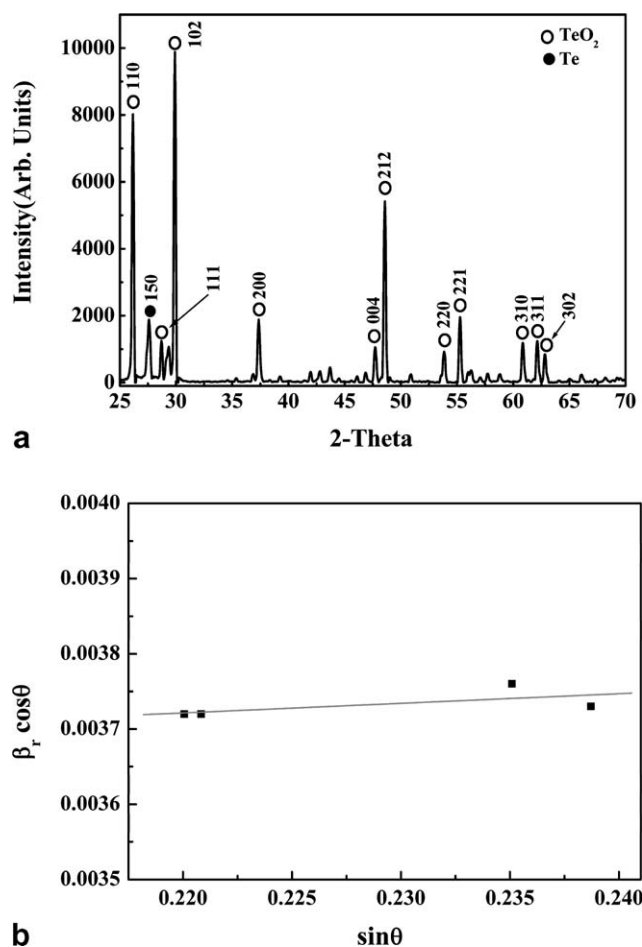


Fig. 3. (a) XRD pattern of the as-produced  $\text{TeO}_2$  nanoparticles. (b) Williamson–Hall plot of  $\beta \cos \theta$  vs  $\sin \theta$  for XRD pattern corresponding to (a).

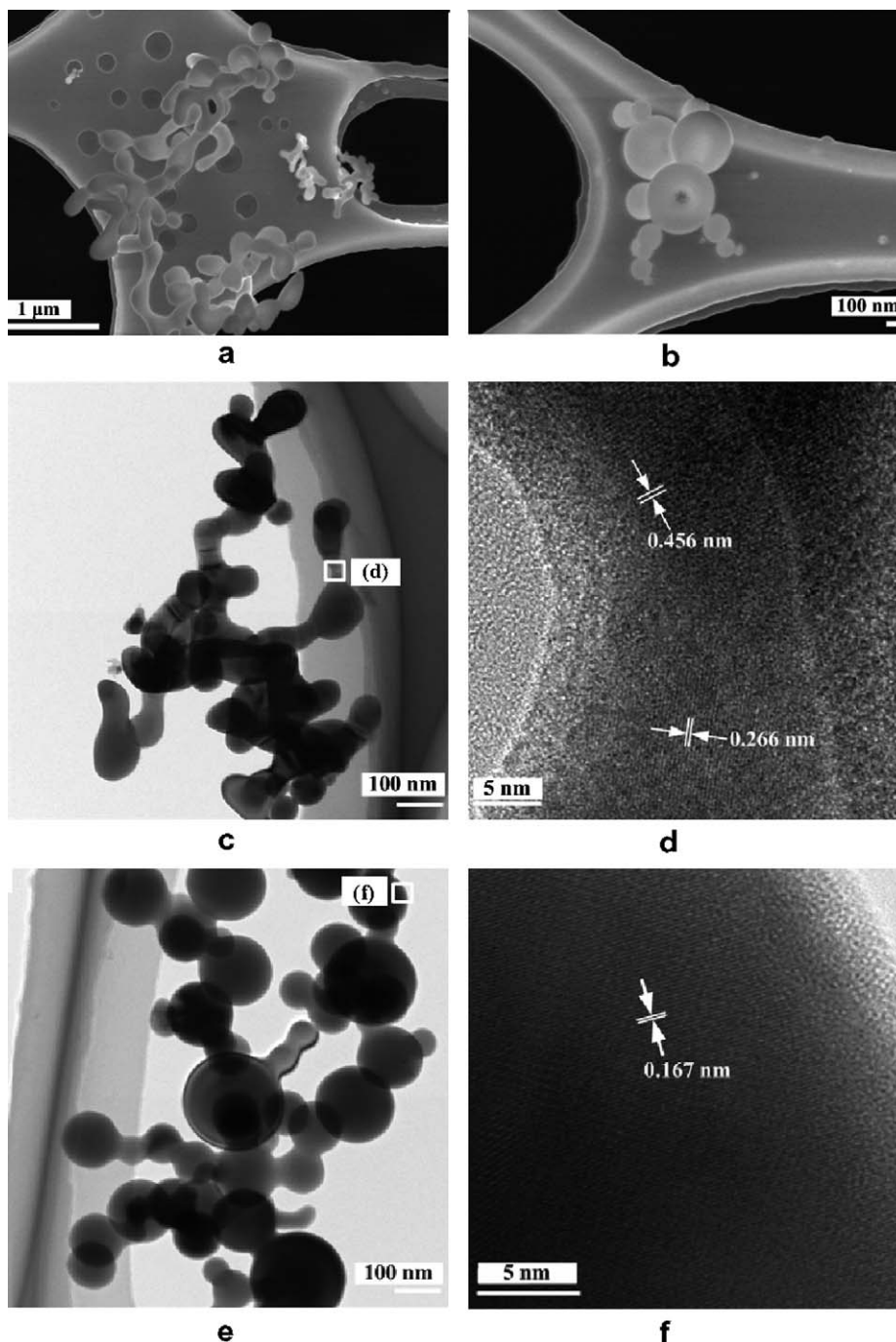


Fig. 4. SEM and TEM images of the as-synthesized  $\text{TeO}_2$  nanoparticles: (a, b) The SEM images showing aggregated and sphere-shaped  $\text{TeO}_2$  particles, respectively. (c) The TEM image corresponding to the SEM image of (a). (d) A close-up image of a rectangular box in (c). (e) The TEM image corresponding to the SEM image of (b). (f) A magnified view of a rectangular box in (d).

plasma flame and a low melting point ( $\sim 1000$  K) of  $\text{TeO}_2$  [2], relatively. However, Fig. 4b shows the  $\text{TeO}_2$  nanoparticles near perfect sphere in the range of 37.5–340 nm. The  $\text{TeO}_2$  nanoparticles with sphere shape were taken from the region away from the plasma flame, a relatively cool region, showing a quenching effect. Fig. 4c is the TEM image of aggregated  $\text{TeO}_2$  particles corresponding to Fig. 4a. Fig. 4d is a magnified view of a part marked with a rectangular box in Fig. 4c, revealing well-ordered individ-

ual layers of 0.456 nm and 0.266 nm thicknesses with high crystallinity, respectively. The findings means that two independent particles are aggregated each other. Fig. 4e shows the TEM image of  $\text{TeO}_2$  nanoparticles with sphere shape corresponding to Fig. 4b. As shown in the SEM image of Fig. 4b, near perfect  $\text{TeO}_2$  spheres were observed. During TEM measurement, however, we observed that  $\text{TeO}_2$  nanoparticles were damaged severely and were aggregated by electron beam. A large  $\text{TeO}_2$  sphere ( $\sim 180$  nm in

diameter) in center part of Fig. 4e was attached with two small TeO<sub>2</sub> spheres due to electron beam. The average particle size measured from Fig. 4e was approximately 108.2 nm consistent with the average particle size estimated from the Williamson–Hall equation in Fig. 3b. Fig. 4f is a magnified view of a rectangular box (d) in Fig. 4e, revealing well-ordered layers of 0.167 nm thickness. In the synthesis method by evaporation of metal in flame, metallic Te may be located at the core of the TeO<sub>2</sub> or form separate particle. From energy dispersive X-ray (EDX) spectrum not shown in this Letter, Te and oxygen species were detected with atomic fraction of 66.6% oxygen and 33.4% tellurium consistently. If the small amount of Te in Fig. 3a is ignored, we expect that the as-produced sample is the oxide particle close to 100%. Therefore, metallic Te is not incorporated into the core of the oxide particle but exists as separate particle.

In order to characterize the surface area and pore distribution properties, the as-produced TeO<sub>2</sub> nanoparticles were analyzed by a nitrogen adsorption method. The as-produced sample had the specific surface area of about 5.75 m<sup>2</sup>/g at  $P/P_0 = 0.2$ , porosity of 53.2%, pore volume of 0.011 cm<sup>3</sup>/g at  $P/P_0 = 0.97$ , and pore size of 7.17 nm. Fig. 5 shows the pore size distribution curve calculated from the desorption branch of nitrogen isotherm by the BJH method using the Halsey equation [17,20]. The TeO<sub>2</sub> powders in Fig. 5 reveal tri-modal pore size distributions consisting of *mesopores* (<20 nm), *macropores* (about 51 nm and about 80 nm). According to Kumer et al. [21], *mesopores* and *macropores* are due to the finer intra-aggregated and the larger intra-aggregated pores, respectively. The inset also reveals the corresponding nitrogen adsorption–desorption isotherms of the sample. According to the Brunauer–Deming–Deming–Teller (BDDT) classification [18], the shape in the inset of Fig. 5 is a combination of types I and IV of adsorption isotherms. At a very-low relative pressure ( $P/P_0 < 0.1$ ), the isotherm exhibits high

adsorption, demonstrating that the TeO<sub>2</sub> powder contains micropores. However, at the relative pressure  $P/P_0$  in the range of 0.82–1.0, there is a close hysteresis loop, which can be observed in the pores with narrow necks and wider bodies such as an ink-bottle, and can be associated with the aggregates of particles.

In summary, TeO<sub>2</sub> nanoparticles have been synthesized by directly heating Te granules in the O<sub>2</sub> microwave-plasma torch-flame at atmospheric pressure. The mean size of the synthesized TeO<sub>2</sub> particles was 108.2 nm observed from the TEM image and was 112.0 nm estimated by the Williamson–Hall plot using XRD data. From the BET measurements, the sample also showed the specific surface area of about 5.75 m<sup>2</sup>/g, porosity of 53.2%, pore volume of 0.011 cm<sup>3</sup>/g, and pore size of 7.17 nm. Although the synthesis approach by the microwave plasma torch in the experiment is not finely controlled, this synthesis method may be suitable for the direct continuous preparation and mass production of TeO<sub>2</sub> nanoparticles.

### Acknowledgements

We acknowledge the financial support from the Nuclear Fusion Research Center (NFRC) in Korea and BK 21 program in part. TEM data were obtained from CCRF in Sungkyunkwan University.

### References

- [1] S. Kitova, V. Rashkova, I. Konstantinov, Vacuum 69 (2003) 405.
- [2] A.C.M. Rodrigues, R. Keding, C. Rüssel, J. Non-Cryst. Solids 273 (2000) 53.
- [3] V.S. Vassilev, Z.G. Ivanova, E.S. Dospeiska, S.V. Boycheva, J. Phys. Chem. Solids 63 (2002) 815.
- [4] R.A.F. El-Mallaway, Tellurite Glasses Handbook: Properties and Data, CRC, Boca Raton, FL, 2002.
- [5] G. Perrin, D. Coutris, J. Phys. Chem. Solids 49 (1988) 1397.
- [6] F. Told, Glastechn. Ber. 33 (1960) 303.
- [7] B. Jeansannetas et al., J. Solid State Chem. 146 (1999) 329.
- [8] A. Pierre, F. Duboudin, B. Tanguy, J. Portier, J. Non-Cryst. Solids 147 (1992) 569.
- [9] S.N.B. Hodgson, L.J. Weng, J. Non-Cryst. Solids 276 (2000) 195.
- [10] K.M. Green, M.C. Borass, P.P. Woskov, G.J. Flores, K. Hadidi, P. Thomas, IEEE Trans. Plasma Sci. 29 (2001) 399.
- [11] W. Lai, H. Lai, S.P. Kuo, O. Tarasenko, K. Levon, Phys. Plasmas 12 (2005) 023501.
- [12] Y.C. Hong, H.S. Uhm, Phys. Plasmas 12 (2005) 053504.
- [13] Y.C. Hong, C.U. Bang, D.H. Shin, H.S. Uhm, Chem. Phys. Lett. 413 (2005) 454.
- [14] Y.C. Hong, H.S. Uhm, Chem. Phys. Lett. 422 (2006) 174.
- [15] D.H. Shin, Y.C. Hong, H.S. Uhm, J. Am. Ceram. Soc. 88 (2005) 2736.
- [16] Y.C. Hong, J.H. Kim, S.C. Cho, H.S. Uhm, Phys. Plasmas 13 (2006) 063506.
- [17] K.S.W. Sing, D.H. Everett, R.A.W. Haul, L. Moscou, R.A. Pierotti, J. Rouquerol, T. Siemieniowska, Pure Appl. Chem. 57 (1985) 603.
- [18] P.A. Thomas, Solid State Phys. 21 (1988) 4611.
- [19] G.K. Williamson, W.H. Hall, Acta Metal. 1 (1953) 22.
- [20] A.W. Adamson, A.P. Gast, Physical Chemistry of Surfaces, John Wiley & Sons, Inc., New York, 1997, p. 599.
- [21] K.N.P. Kumer, J. Kumer, K. Keizer, J. Am. Ceram. Soc. 77 (1994) 1396.

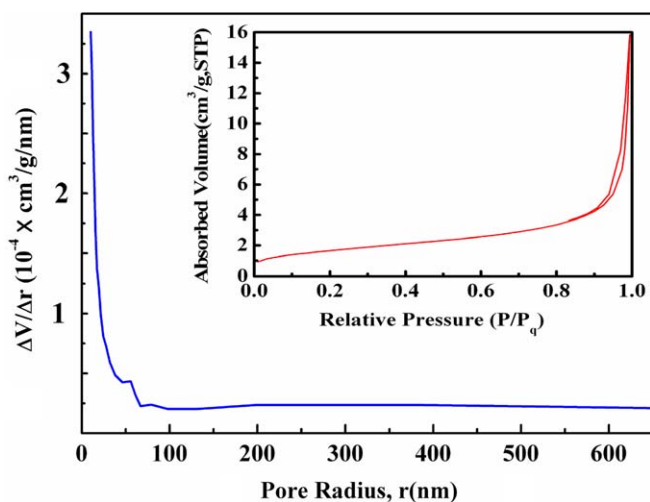


Fig. 5. The pore size distribution curve and the corresponding nitrogen isotherms (inset) of the as-produced samples.